Numerical modelling of multi-component mass transport in a permafrost-impacted groundwater flow system

John Molson[1], Aaron Mohammed[2] & Mario Schirmer[3]

[1]*Department of Geology & Geological Engineering, Université Laval, Québec City, Québec, Canada*

[2]*Department of Earth and Environmental Sciences, Syracuse University, New York, United States*

[3]*Department of Water Resources and Drinking Water, Eawag - Swiss Federal Institute of Aquatic Science and Technology*

ABSTRACT

A 3D numerical model has been developed to simulate groundwater flow, heat transport, and the transport and fate of reactive organic contaminants in a thawing permafrost environment. Insight is needed under such conditions as the climate warms and northern economic development accelerates, increasing the risk of groundwater resource contamination. The model includes coupled density-dependent groundwater flow, advective-conductive heat transport with latent heat and freeze/thaw, and advective-dispersive multi-component reactive mass transport. The reactive transport component can account for multi-component aerobic and anaerobic biodegradation with multiple electron acceptors and microbial growth/decay, with temperature-dependent reaction rates governed by Monod kinetics. Model functionality and performance are tested on a 2D vertical-plane conceptual model of a field-scale cryo-hydrogeological system including thawing discontinuous permafrost and an evolving groundwater flow system. The test case includes a surface gasoline spill containing dissolved benzene, toluene, ethylbenzene, and xylene (BTEX), and a bulk residual component, migrating within a shallow aquifer and undergoing aerobic biodegradation. The presence of thawing permafrost, with associated effects on ice-fraction dependent relative permeability, strongly modulated subsurface hydraulic properties and connectivity, with subsequent changes to groundwater flow and mass transport pathways. Results show how evolution of the dissolved BTEX component plumes is controlled not only by the permafrost-impacted flow system, but also by the interacting thermal and chemical controls on overall biodegradation kinetics as the system evolves during permafrost thaw.

1 INTRODUCTION

As the climate warms and northern development accelerates, risks of contaminant spills in thawing permafrost environments will increase, posing risks to groundwater resources (Wiebe et al. 2023). Hydrocarbon spills such as gasoline and diesel fuel are a particular threat due to their mobility and toxicity at low concentrations.

While much is known about the fate of dissolved hydrocarbons in aquifer systems within temperate climates, much less is known about their behavior and potential for degradation in cold regions. In permafrost environments, frozen ground can affect recharge and discharge zones, and can change flow rates and contaminant pathways. Colder temperatures can also affect component solubilities and can reduce microbial activity, reducing biodegradation rates. The processes are complex and highly non-linear, and are difficult to interpret or predict without advanced numerical models.

Many numerical models have been developed for simulating coupled groundwater flow and heat transport in cold regions (e.g., see reviews by Lamontagne-Hallé et al. 2020 and Grenier et al. 2018). Frampton and Destouni (2015) use numerical flow modelling to investigate travel times in degrading permafrost environments, and advanced coupled models for simulating heat and reactive mass transport in cold regions have also recently appeared (Ramezanzadeh et al. 2023; Mohammed et al. 2021; Yi et al. 2021a,b; Barkow et al. 2020; Lessels et al. 2015). Applications of cryo-hydrogeological models for simulating aerobic or anaerobic biodegradation of organic contaminants in permafrost environments have not yet been published.

In this paper, we present a newly-developed finite element numerical model, SMOKER-BIO, for simulating density-dependent groundwater flow, heat transport and multi-component reactive mass transport under aerobic or anaerobic biodegradation, including temperature-dependent reaction rates. The numerical model is applied to a 2D conceptual model of a gasoline spill in a shallow aquifer containing thawing discontinuous permafrost. The source is a 3-component gasoline spill zone composed of dissolved benzene, a lumped component of toluene, ethylbenzene and xylene (together referred to as BTEX), and a bulk residual gasoline component.

Evolution of the flow system, temperature distribution and dissolved plumes is simulated over time, until complete permafrost thaw.

2 NUMERICAL MODEL

The new 3D SMOKER-BIO model is a hybrid version of the BIONAPL/3D code for groundwater flow and multi-component reactive mass transport (Molson 2022), coupled with the HEATFLOW/SMOKER code for heat transport and permafrost thaw (Molson and Frind 2023). Field applications of the original codes include Freitas et al. (2010), Dagenais et al. (2020) and Liu et al. (2022).

https://doi.org/10.52381/ICOP2024.126.1

SMOKER-BIO couples a 3D transient groundwater flow equation with an advective-conductive heat transport equation, and with multiple advective-dispersive-reactive mass transport equations, one for each component and one for each electron acceptor, and includes microbial growth and decay. The equations are briefly reviewed below. For simplicity the groundwater flow equation is omitted.

2.1 Governing equations

The governing equation for heat transport is written as:

$$\frac{\partial (C_o T)}{\partial t} = -\frac{\partial}{\partial x_i}\left(\theta S_w c_w \rho_w v_i T\right) + \frac{\partial}{\partial x_i}\left(\left(\lambda + \theta S_w c_w \rho_w D_{ij}\right)\frac{\partial T}{\partial x_j}\right) \quad (1)$$

where T is the temperature (°C), θ is the porosity, S_w the unfrozen water saturation (-), c_w the specific heat (J/kg/K), ρ_w the fluid density (kgm^{-3}), v_i the pore velocity (ms^{-1}), λ is the bulk thermal conductivity of the porous medium (J/m/s/K), D_{ij} the hydrodynamic dispersion coefficient (m^{2}s^{-1}), t is time (s) and x_{ij} are the spatial coordinates (m). In Eq. 1, the temperature-dependent heat capacity C_o (Jm^{-3} K^{-1}), is defined as:

$$C_o = \theta S_w c_w \rho_w + \theta S_i c_i \rho_i + (1-\theta) c_s \rho_s + \theta \rho_i L \left(\frac{\partial S_w}{\partial T}\right) \quad (2)$$

where *L* is the latent heat of water (J/kg) and the subscripts *w*, *i* and *s* refer to the water, ice and solids, respectively. The unfrozen water saturation S_w in the above equations is here replaced by the temperature-dependent function *Wu*, which in turn is used to define an exponential relative permeability function $k_r(T)$ which accounts for pore blockage from ice formation. Further details are provided in Molson and Frind (2023).

The governing equation for advective-dispersive-reactive mass transport can be written as:

$$R\frac{\partial C^\alpha}{\partial t} = \frac{\partial}{\partial x_i}\left[D_{ij}\frac{\partial C^\alpha}{\partial x_j}\right] - v_i\frac{\partial C^\alpha}{\partial x_i} - \lambda^\alpha_{BIO} C^\alpha \quad (3)$$

where C^α is the concentration of component α (kgm^{-3}), R is the retardation factor to account for sorption, and λ^α_{BIO} is the effective biodegradation rate (s^{-1}), given by:

$$\lambda^\alpha_{BIO} = \sum_{n=1}^{N_A}\left[\tilde{k}^{\alpha,n} M^n \left(\frac{1}{K_C{}^{\alpha,n} + C^\alpha}\right)\bullet\left(\frac{A^n}{K_A{}^{\alpha,n} + A^n}\right)\right] \quad (4)$$

where $\tilde{k}^{\alpha,n}$ is the temperature-dependent maximum substrate utilization rate (kg$_S$kg$_M$$^{-1}$day^{-1}), A^n is the concentration of electron acceptor n (kgm^{-3}), M^n is the microbe concentration (kgm^{-3}), $K_C{}^{\alpha,n}$ is the organic half-utilization-rate concentration (kgm^{-3}), $K_A{}^{\alpha,n}$ is the electron acceptor half-utilization-rate concentration (kgm^{-3}) and N_A is the number of electron acceptors.

Following Mohammed et al. (2021), the temperature-dependency of the maximum utilization rate in Eq. 4 is expressed using a power function as:

$$\tilde{k}^{\alpha,n} = k^{\alpha,n} \cdot Q_{10}{}^{0.1\cdot(T-T*)} \quad (5)$$

where $k^{\alpha,n}$ is the intrinsic maximum degradation rate at the reference temperature T*, and Q_{10} is the rate increase factor for each 10 °C increase in temperature. While Eq. 5 was used by Mohammed et al. (2022) for DOC reactions, lacking specific temperature-dependent biodegradation rates for BTEX components, we adopt it here for simplicity. We note that in SMOKER-BIO, Eq. 5 can be easily replaced in a single line of code as more reliable rate laws become available.

Eq. 3 for each component is coupled with corresponding equations for transport and consumption of each electron acceptor:

$$R\frac{\partial A^n}{\partial t} = \frac{\partial}{\partial x_i}\left[D_{ij}\frac{\partial A^n}{\partial x_j}\right] - v_i\frac{\partial A^n}{\partial x_i} - \lambda^n_{BIO} A^n \quad (6)$$

where λ^n_{BIO} is the electron acceptor consumption rate (s^{-1}) which can be written as:

$$\lambda^n_{BIO} = \sum_{\alpha=1}^{Nc}\left[\tilde{k}^{\alpha,n} M^n X^{\alpha,n}\left(\frac{C^\alpha}{K_C{}^{\alpha,n} + C^\alpha}\right)\bullet\left(\frac{1}{K_A{}^{\alpha,n} + A^n}\right)\right] \quad (7)$$

where $X^{\alpha,n}$ is the stoichiometric ratio of the mass of electron acceptor consumed per mass of organic consumed (kg/kg) and N_c is the number of components. A single microbial population of concentration M^n is associated with each electron acceptor, and can grow or decay depending on the availability of substrates and electron acceptors. For simplicity, we neglect inhibition. See Molson (2022) for further details on the governing equations.

2.2 Solution approach

The groundwater flow, heat and mass transport equations are discretized using a Galerkin finite element scheme with Picard iteration to handle the non-linearities including temperature-dependent fluid density, viscosity, relative permeability (due to ice fraction), and the maximum substrate utilization rates $\tilde{k}^{\alpha,n}$. The bulk thermal conductivity, aquifer heat capacity, unfrozen water saturation and relative permeability are also temperature-dependent functions (see Molson and Frind, 2023).

Under Monod kinetics, the substrate and electron acceptor reaction rates (λ^α_{BIO} and λ^n_{BIO} in Eq. 4 and 7) are also non-linear and depend on the relative concentrations of the organic substrates, electron acceptors and microbial populations. Full details are provided in Molson and Frind (2023) and Molson (2022). While fully 3D, the model is here applied in a 2D vertical plane only.

3 MODEL APPLICATION

3.1 Conceptual model

The 2D vertical-plane conceptual model (Figure 1) is based on a reference scenario presented in Molson et al. (2002) in which a residual ethanol-free gasoline is dissolving into a shallow sandy aquifer under uniform temperature conditions. The changes for the current system include: 1) an increase in the aquifer thickness from 10 to 50 m to more realistically allow the addition of a permafrost layer, 2) replacement of the imposed flux condition at the left boundary by a fixed head boundary to allow a natural variation in flux depending on the freeze/thaw state, 3) replacement of the dissolving non-aqueous phase liquid (NAPL) source zone by an initial condition of dissolved-phase BTEX concentrations (avoiding the need for defining temperature-dependent NAPL dissolution rates which are not well known), 4) the addition of discontinuous permafrost within a horizontal silt layer, and 5) addition of temperature-dependent reaction rates.

The background sand aquifer is assumed isotropic with an intrinsic (unfrozen) hydraulic conductivity of 1e-5 m/s and a porosity of 0.35. Consistent with conditions at the Umiujaq field site (Nunavik, Québec, Canada; Dagenais et al. 2020), the discontinuous permafrost is set within a 20 m thick silt layer (see Figure 1 and Table 1 for all physical parameters).

The conceptual model includes a 3-component dissolved gasoline source zone, a single electron acceptor of oxygen, and a single aerobic microbial population. As applied in Molson et al. (2002), the three gasoline source components are i) benzene, ii) a lumped component representing toluene, ethylbenzene and xylene (TEX), and iii) a bulk component representing all (heavier) remaining hydrocarbons in the gasoline (Table 2; hereinafter, this source is simply referred to as BTEX).

Table 1. Flow, heat and component-independent transport parameter values assumed in the simulations.

Parameter	Value
Hydraulic conductivity K *	1e-5, 1e-6 m/s
Porosity*	0.35, 0.2
Specific storage	0.0 m^{-1}
Dry bulk density (ρ_b)	1700 kg/m^3
Thermal conductivity of water λ_w	0.58 J/m/s/K
Thermal conductivity of ice λ_i	2.14 J/m/s/K
Thermal conductivity of solids λ_s	2.0 J/m/s/K
Specific heat of water	4174 J/kg/K
Specific heat of ice	2108 J/kg/K
Specific heat of solids	800 J/kg/K
Density of solids	2630 kg/m^3
Dispersivities (α_L, α_{TV})	1.0, 0.01 m
Freezing function p,q**	0.1, 5.0
Latent heat of water	3.34e5 J/kg

* Intrinsic K (at T > 0°C): background, silt layer
** See Eq 19 and 24 in Molson and Frind (2023)

Table 2. Reaction stoichiometry and mass ratios used in the multi-component simulations (see Molson et al. 2002).

Gasoline Component	Reaction Stoichiometry	O_2:Substrate Mass Ratio $\chi^{\alpha,n}$ (kg_A/kg_S)
Benzene	$C_6H_6 + 15/2\ O_2 \rightarrow 6CO_2 + 3H_2O$	3.08
TEX	$C_7H_8 + 9O_2 \rightarrow 7CO_2 + 4H_2O$	3.13
Bulk	$C_8H_{18} + 25/2\ O_2 \rightarrow 8CO_2 + 9H_2O$	3.5

3.2 Domain, boundary and initial conditions

The 2D model domain is 400 m long by 50 m deep (Figure 1) which is discretized using a 1 m x 1 m square hexahedral mesh (the grid is 1 element wide in the transverse direction), for a total of 20,000 elements. A mean annual recharge rate of 200 mm/yr is applied across the top watertable boundary, a fixed head of 55 m is applied across the left inflow boundary, and a head of 50 m is applied at the right outflow boundary. The base is assumed impermeable.

For heat transport, the watertable is assumed to remain at a yearly average temperature of +1 °C over the 30-year simulation period, while a zero-gradient temperature condition is applied at the left and right, allowing advective energy inflow and outflow, respectively. A constant geothermal flux of 0.032 $J/s/m^2$ is applied at the base (Figure 1).

For mass transport, zero-gradient concentration conditions are applied for all components at the left, right and bottom, while Dirichlet (type-1) constant concentrations are applied at the top, representing background recharge water (i.e., BTEX concentrations of 0.0 mg/L and a dissolved oxygen concentration of 3.8 mg/L). Note that the initial background oxygen concentration is assumed less than its solubility due to oxidation of natural organic carbon.

The initial temperature of the discontinuous permafrost layer is assumed at -5 °C while an initial background temperature of +1 °C is applied everywhere else. For simplicity in this test example, a separate initial equilibration period is not included, and the model is run until all permafrost is thawed and the flow system has stabilized.

The aquifer is assumed initially uncontaminated with c = 0 for all components, and with background oxygen and microbe concentrations of 3.8 mg/L and 3.0 mg/L, respectively. Initial dissolved phase concentrations (C_o) for the BTEX and bulk components in the source zone (Table 3) are based on their pure phase solubilities and mole fractions of a standard gasoline (after Molson et al. 2002).

For the temperature-dependent rate expression of Eq. 5, we assume Q_{10} = 2.0 and a reference temperature T* = 10 °C. The effective biodegradation reaction rate thus decreases by a factor of 2 between 10 °C (where the reference rate applies) and 0 °C. Below 0 °C the reaction rate is assumed zero.

A uniform time step of 0.5 days was used for all simulations for which convergence was usually attained within 2–3 iterations at each time step. The model was run to

11,000 days (~30 years), by which time the permafrost had completely thawed.

Table 3. Reactive transport parameters and source concentrations assumed in the simulations for each component (from Molson et al. 2002).

Parameter	Benzene	TEX	Bulk
R (-)	1.1	2.0	2.8
D* (m^2/s) (1)	7.7e-10	6.2e-10	6.2e-10
$k^{\alpha,n}$ ($kg_S kg_M^{-1} d^{-1}$)	1.0	1.0	0.1
$K_C^{\alpha,n}$ (kg/m^3)	0.002	0.002	0.002
$K_A^{\alpha,n}$ (kg/m^3)	0.002	0.002	0.002
$X^{\alpha,n}$ (kg_A/kg_S)	3.08	3.13	3.5
C_o (g/L) (source)	0.0320	0.0455	0.0165

(1) D*: effective diffusion coefficient

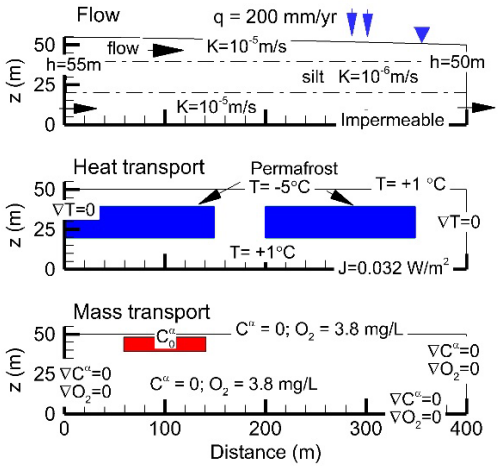

Figure 1. Simulation domain for the coupled reactive transport system showing boundary and initial conditions for flow, heat and mass transport.

3.3 Assumptions and limitations

The main assumptions in the simulations presented here include a fully saturated isotropic 2D porous medium, local thermal equilibrium, and linear equilibrium sorption. While the model can account for multiple electron acceptors, the reaction kinetics in this example assume only oxygen is present, they neglect inhibition, and assume the BTEX components degrade under complete mineralization (to CO_2 and H_2O). The microbial population is assumed immobile, and assumed inactive at T < 0 °C, and there is no effect of component concentrations on the freeze/thaw behaviour of groundwater. We note that by design, the time scale of permafrost thaw in this example (~30 years) is relatively fast, on the same order as the plume evolution, which helps identify process interaction and model functionality more rapidly. The example is not a verification of the model but a conceptual case only.

4 Simulation Results

Simulation results are provided in the vertical plane for the base case Scenario 1 with temperature-dependent reaction rates ($\tilde{k}^{\alpha,n}$), after 10 yrs and 30 yrs, respectively, in Figures 2 and 3. The flow system is illustrated as hydraulic head contours and using flow lines calculated from particle tracking with Tecplot©. Outlines of the three substrates (benzene, TEX and Bulk components), and of dissolved oxygen and the microbe population, are shown using concentration contours, with oxygen appearing as a depletion plume.

Acknowledging the simplifications of this example, model functionality with respect to coupling of the governing physical processes is nevertheless well illustrated.

Migration of the gasoline components is primarily driven by the background flow system, which at 10 yrs is still diverting around the two thawing permafrost zones (Figure 2) due to their lower relatively permeability. While several flow lines originating from the top left of the upper aquifer remain in the shallow zone above both permafrost blocks, others divert downward through the intervening talik (unfrozen zone within the silt), where they pass below the base of the right permafrost block.

While only representing a snapshot of the transient flow field, the particle tracks and time markers show advective travel times through the shallow unfrozen zone of about 20–30 yrs. Very low flow velocities through the permafrost lead to much longer travel times. Note that velocities also remain relatively low through the talik since the intrinsic (unfrozen) hydraulic conductivity of the silt layer remains 10 times less than the background aquifer. The presence of permafrost reduces the hydraulic conductivity much further.

These perturbations in the flow system due to the presence of (thawing) permafrost have subsequently affected evolution of the gasoline component plumes. Up to about 10 yrs, for example (Figure 2), the lower relative permeability of the permafrost tended to force the plumes to remain in the shallow thawed zone, rather than migrate and disperse deeper into the aquifer. At 10 yrs, the benzene plume, being the most mobile component, has reached the intervening talik, and begins to split, with one portion continuing in the shallow thawed zone while another follows the flow downward through the talik and eventually into the thawed zone below the right permafrost block.

Due to their higher retardation, the TEX and Bulk component plumes lag respectively behind the benzene plume (Figure 2). The corresponding dissolved oxygen plume, being non-retarded and depleted due to consumption during biodegradation of the hydrocarbons, migrates slightly ahead of the benzene plume, also showing a splitting effect through the talik due to the flow system. The tail of the oxygen depletion plume more closely follows the TEX and Bulk component plumes, the oxidation of which also consumes oxygen once the benzene plume has passed. Growth of the microbe population follows the BTEX plumes and oxygen depletion plumes.

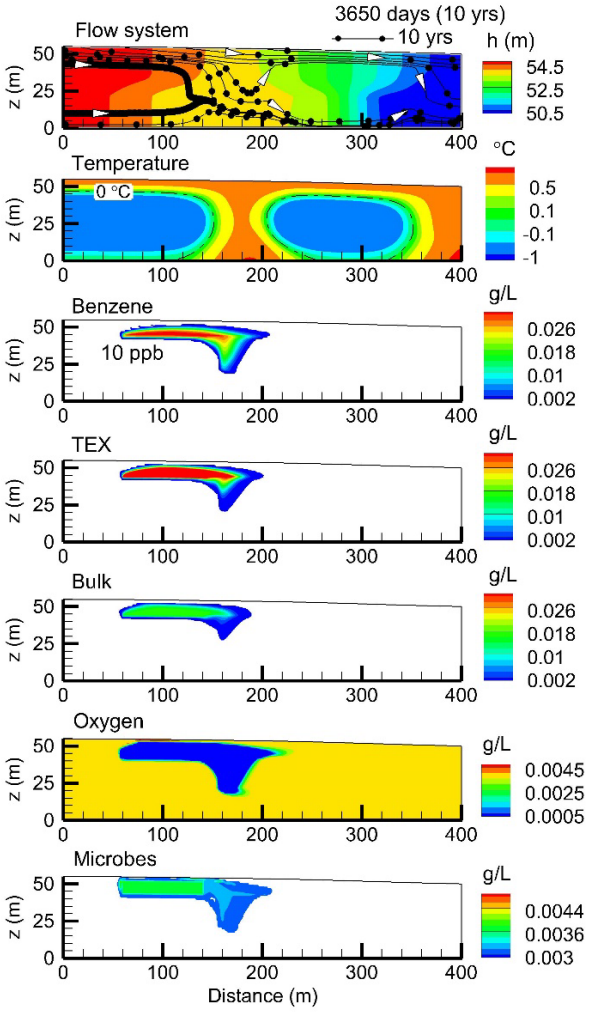

Figure 2. Base case (Scenario 1) simulation at 3650 days(10 yrs) with temperature-dependent reaction rates $\tilde{k}^{\alpha,n}$ (Eq. 5), showing the flow system, temperature, component concentrations, and dissolved oxygen and microbe concentrations. Time marker interval in the flow system is 5 yrs. Vertical exaggeration is 1.5x.

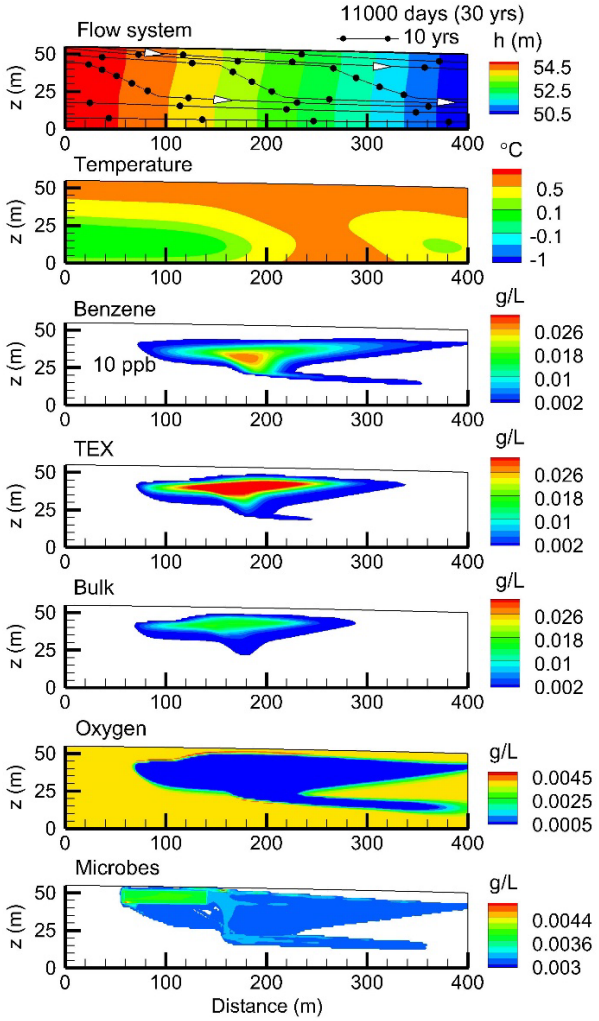

Figure 3. Base case (Scenario 1) simulation at 11,000 days (~30 yrs) with temperature-dependent reaction rates $\tilde{k}^{\alpha,n}$ (Eq 5), showing the flow system, temperature, component concentrations, and dissolved oxygen and microbe concentrations. Time marker interval in the flow system is 5 yrs. Vertical exaggeration is 1.5x.

Plume behavior with sorption, and with multi-component reactions in the presence of thawing permafrost, thus depends strongly on the transient flow system, notwithstanding the lower reaction rates due to colder temperatures. Different parts of each component plume, which are migrating at different velocities, respond differently to the local transient conditions.

By 30 yrs, the permafrost has completely thawed and the flow system has equilibrated, with flow dominantly in the upper and lower aquifers separated by the now unfrozen but still less permeable silt layer (Figure 3). Maximum travel times have decreased to about 60 yrs for flow passing through the silt. Of particular note is the asymmetrical shape of the benzene plume due to remnant effects of the talik and permafrost, with a relatively more elongated upper portion of the plume and a lower plume finger migrating in the lower aquifer. In comparison, due to their slower migration rates, the TEX and bulk component plumes show somewhat less asymmetry, having felt more of the recovered late-time flow system following permafrost thaw. In the oxygen depletion and microbial growth plumes, remnant plume 'fingers' are also evident within the lower aquifer.

To compare the effect on plume concentrations of the lower reaction rates with lower temperatures (Eq. 5), a second simulation (Scenario 2) was run with no temperature effect on the reaction rates, thus assuming the reference rates at 10 °C (while retaining the same conceptual model). These two scenarios are compared in Figures 4 and 5 as differences in concentration (Scenario 1 – Scenario 2) at 10 and 30 yrs, respectively.

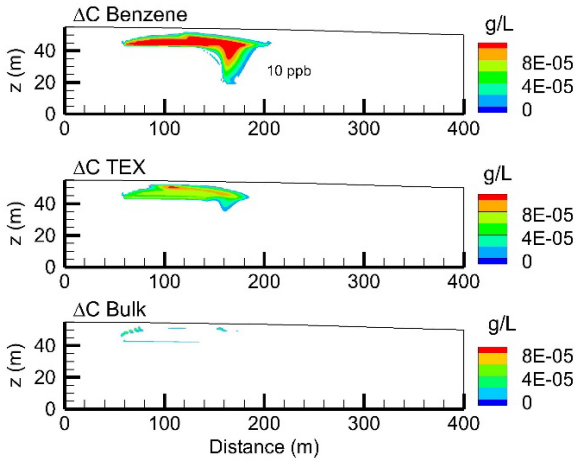

Figure 4. Concentration differences (ΔC) at 10 yrs, where ΔC = (Scenario 1 (temperature-dependent rates $\tilde{k}^{\alpha,n}$) – Scenario 2 (reference rates at 10 °C)), for B, TEX and Bulk components. Limit contour is 10 ppb for each component. Vertical exaggeration is 1.5x.

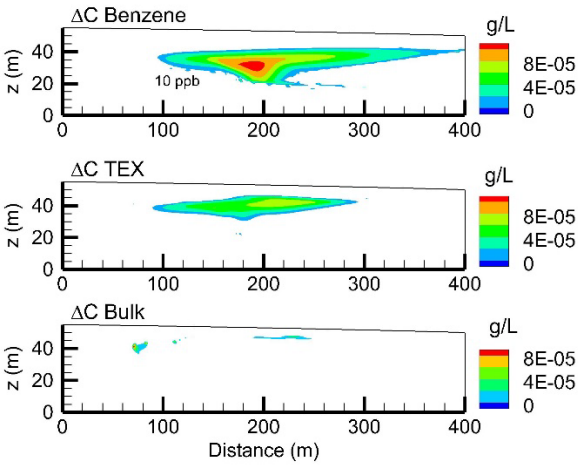

Figure 5. Concentration differences (ΔC) at 30 yrs, where ΔC = (Scenario 1 (temperature-dependent rates $\tilde{k}^{\alpha,n}$) – Scenario 2 (reference rates at 10 °C)), for B, TEX and Bulk components. Limit contour is 10 ppb for each component. Vertical exaggeration is 1.5x.

Concentrations of the gasoline components are higher with the temperature-dependent rates in Scenario 1 (hence positive differences in Figures 4 and 5) since the reaction rates are assumed up to 2x lower at temperatures near 0 °C (and reactions are assumed to cease at 0°C). However, the maximum differences for benzene are only on the order of 100 ppb (1e-4 g/L), and even less for TEX and the bulk components. The effects of temperature on reaction rates, even assuming a maximum 2x decrease from 10 °C to 0 °C, are somewhat attenuated since the effective reaction rates (Eq. 4 and 7 for the substrates and oxygen, respectively), even in the reference 10°C case, remain oxygen-limiting.

Oxygen limitations (and in general for any electron acceptor) arise from limited dispersive mixing and due to low background oxygen concentrations. Dispersive mixing is restricted by the low dispersivities (Table 1; in particular the transverse vertical dispersivity of 0.01 m), by the assumed homogeneous layers of the porous medium, and by the underlying low permeability permafrost. Although not included in this study, the higher solubility of oxygen at lower temperatures could further reduce the impact of lower reaction rates at lower temperatures.

Compared to benzene, the relative impact of temperature on plume concentrations decreases for TEX, and even further for the bulk component, because of lower intrinsic degradation since oxygen limitations increase for retarded plumes, and because the maximum utilization rate $\tilde{k}^{\alpha,n}$ is lowest for the bulk component (Table 3).

5 CONCLUSIONS

A 3D finite element numerical model has been developed for simulating coupled groundwater flow, heat transport with freeze/thaw, and multi-component advective-dispersive reactive transport. The model was applied and tested in a 2D vertical plane domain including thawing discontinuous permafrost, three dissolved gasoline components, and with dissolved oxygen as an electron acceptor.

Transport and fate of the dissolved gasoline components followed typical behavior associated with electron acceptor-limited biodegradation in more temperate climates, including plume separation due to differing retardation factors among the components, and the sequential consumption of dissolved oxygen. In this context of plume evolution in cold climates, which included discontinuous permafrost, the most significant effect on the hydrocarbon plumes was due to the perturbed flow system impacted by permafrost. In particular, flow deviation around the relatively lower permeability permafrost zones, and recovery of the flow system during permafrost thaw, was a controlling factor. While the lower-K silt layer had a persistent effect on the flow system, the presence of permafrost within the silt had an even greater influence, especially at early time when permafrost temperatures and the associated relative permeabilities of the silt, were lowest.

Effects of lower temperatures on reducing reaction rates were somewhat attenuated in this case since the system was effectively oxygen-limited, even without a temperature effect on the reaction rates. Temperature-dependent reaction rates might be expected to have greater effect under multi-electron acceptor systems (where availability of

specific electron-acceptors would be offset by the presence of others), with higher dispersive mixing, and with a seasonally-varying active layer.

Further testing of the model is underway under these more complex conditions, including under transient ground surface temperatures and benchmarking against other codes. Such models should also be tested against real field spills and using component-specific reaction rates determined under cold temperature conditions.

6 REFERENCES

Barkow, I.S., Oswald, S.E., Lensing, H-J., and Munz, M. 2020. 'Seasonal dynamics modifies fate of oxygen, nitrate, and organic micropollutants during bank filtration—temperature-dependent reactive transport modeling of field data', *Environmental Science and Pollution Research* 28, pp. 9682–9700. doi:10.1007/s11356-020-11002-9.

Dagenais, S., Molson, J., Lemieux, J.-M., Fortier, R., and Therrien, R. 2020. 'Coupled cryo-hydrogeological modelling of permafrost dynamics near Umiujaq (Nunavik, Canada)', *Hydrogeology Journal* 28, pp. 887–904. doi:10.1007/s10040-020-02111-3.

Frampton, A. and Destouni, G. 2015. 'Impact of degrading permafrost on subsurface solute transport pathways and travel times', *Water Resources Research* 51(9), pp. 7680–7701, doi:10.1002/2014WR016689.

Freitas, J., Mocanu, M., Zoby, J.L.G., Molson, J., and Barker, J. 2010. 'Migration and fate of ethanol-enhanced gasoline in groundwater: A modelling analysis of a field experiment', *Journal of Contaminant Hydrology* 119 (25–43), doi:10.1016/j.jconhyd.2010.08.007.

Grenier, C., Anbergen, H., Bense, V., Chanzy, Q., Coon, E., Collier, N., et al. 2018. 'Groundwater flow and heat transport for systems undergoing freeze-thaw: Intercomparison of numerical simulators for 2D test cases', *Advances in Water Resources* 114, pp. 196–21. Available at: https://doi.org/10.1016/j.advwatres.2018.02.001.

Lamontagne-Hallé, P. McKenzie, J.M., Kurylyk, B.L., Molson, J., and Lyon, L.N. 2020. 'Guidelines for cold-regions groundwater numerical modeling', *WIREs Water* 7, e1467. doi:10.1002/wat2.1467.

Lessels, J.S. Tetzlaff, D., Carey, S.K., Smith, P., and Soulsby, C. 2015. 'A coupled hydrology-biogeochemistry model to simulate dissolved organic carbon exports from a permafrost-influenced catchment', *Hydrological Processes* 29(26), pp. 5383–5396. doi:10.1002/hyp.10566.

Liu, W., Fortier, R., Molson, J., and Lemieux, J.-M. 2022. 'Three-dimensional numerical modeling of cryo-hydrogeological processes in a river-talik system in a continuous permafrost environment', *Water Resources Research* 58, https://doi.org/10.1029/2021WR031630.

Mohammed, A.A., Bense, V.F., Kurylyk, B.L., Jamieson, R.C., Johnston, L.H., and Jackson, A.J. 2021. 'Modeling reactive solute transport in permafrost-affected groundwater systems', *Water Resources Research* 57, doi:10.1029/2020WR028771.

Mohammed, A.A., Guimond, J.A., Bense, V.F., Jamieson, R.C., McKenzie, J.M., and Kurylyk, B.L. 2022. 'Mobilization of subsurface carbon pools driven by permafrost thaw and reactivation of groundwater flow: a virtual experiment'. *Environmental Research Letters* 17(12), 124036.

Molson, J.W., Barker, J., Frind, E.O., and Schirmer, M. 2002. 'Modelling the impact of ethanol on the persistence of benzene in gasoline-contaminated groundwater', *Water Resources Research* 38(1), pp. 4-1–4-12.

Molson, J.W. and Frind, E.O. 2023. *HEATFLOW-SMOKER User Guide, Density-dependent flow and advective-dispersive transport of mass, thermal energy or residence time in 3D porous* or discretely-fractured porous media. Version 5.0. Québec City, Québec, and Waterloo, Ontario, Canada: Université Laval and University of Waterloo.

Molson, J.W. 2022. *BIONAPL/3D User Guide, A 3D coupled flow and multi-component NAPL dissolution and reactive transport model*. Québec City, Québec, and Waterloo, Ontario, Canada: Université Laval and University of Waterloo.

Ramezanzadeh, M., Slowinski, S., Rezanezhad, F., Murr, K., Lam C., Smeaton, C., Alibert, C., Vandergriendt, M., and Cappellen, V.P. 2023. 'Effects of freeze-thaw cycles on methanogenic hydrocarbon degradation: Experiment and modeling' *Chemosphere* 325.

Yi, X., Su, D., Bussière, B., and Mayer, K.U. 2021a. 'Thermal-hydrological-chemical modeling of a covered waste rock pile in a permafrost region', *Minerals* 11(6), p. 565. doi:10.3390/min11060565.

Yi, X., Su, D., Seigneur, N., and Mayer, K.U. 2021b. 'Modeling of thermal-hydrological-chemical (THC) processes during waste rock weathering under permafrost conditions', *Frontiers in Water* 3, 645675. doi:10.3389/frwa.2021.645675.

Wiebe, A.J., McKenzie, J.M., Hamel, E., Rudolph, D., Mulligan, B., and de Grandpré, I. 2023. 'Groundwater vulnerability in the Yukon and Northwest Territories, Canada', *Hydrogeology Journal*. doi:10.1007/s10040-023-02720-8.